

# Production of $\phi\Lambda$ , $D_s^{*-}\Lambda_c^+$ , and $J/\psi\Lambda$ in kaon-induced reactions off the nucleon

Sang-Ho Kim<sup>1,\*</sup>

<sup>1</sup>*Department of Physics and Origin of Matter and Evolution of Galaxies (OMEG) Institute, Soongsil University, Seoul 06978, South Korea*

(Dated: February 3, 2026)

We investigate the reaction mechanism of strangeness production in  $K^-p \rightarrow \phi\Lambda$  within a hybrid Regge approach, taking into account  $t$ -channel  $K$ - and  $K^*$ -Reggeon exchanges. We present results for the total cross section,  $t$ -dependent differential cross sections, and spin-density matrix elements (SDMEs), and compare them with the available experimental data. We find that  $K^*$ -Reggeon exchange provides the dominant contribution, while  $K$ -Reggeon exchange remains nonnegligible, particularly in describing the SDMEs. In contrast, the  $s$ -channel  $\Lambda$  and  $u$ -channel nucleon exchanges are negligible. To obtain reliable predictions for the open-charm reaction  $K^-p \rightarrow D_s^{*-}\Lambda_c^+$ , we employ a Quark–Gluon String Model (QGSM)-motivated Regge framework that incorporates both pseudoscalar- and vector-Reggeon exchanges. Within this framework, the Regge trajectories  $\alpha(t)$  and energy-scale parameters  $s_0$  are determined consistently, thereby constraining the model and reducing theoretical ambiguities. For the hidden-charm reaction  $K^-p \rightarrow J/\psi\Lambda$ , we use the same quark-level diagrammatic correspondence. The total cross sections for  $K^-p \rightarrow D_s^{*-}\Lambda_c^+$  and  $K^-p \rightarrow J/\psi\Lambda$  are suppressed by approximately 5–6 and 8–9 orders of magnitude, respectively, compared with that for  $K^-p \rightarrow \phi\Lambda$ . We also examine possible  $s$ -channel contributions from the hidden-charm pentaquark states with strangeness,  $P_{cs}(4337)^0$  and  $P_{cs}(4459)^0$ , to both  $D_s^{*-}\Lambda_c^+$  and  $J/\psi\Lambda$  production.

## I. INTRODUCTION

Open- and hidden-charm production constitute central topics in current hadron-physics programs at the PANDA experiment at FAIR (Facility for Antiproton and Ion Research) [1] and at J-PARC (Japan Proton Accelerator Research Complex) [2]. At PANDA, the high-intensity antiproton beam with momenta up to 15 GeV/c will enable systematic investigations of charm dynamics covering open-charm processes such as  $\bar{p}p \rightarrow D\bar{D}^{(*)}$ ,  $\Lambda_c\bar{\Lambda}_c^{(*)}$ ,  $\Sigma_c\bar{\Lambda}_c^{(*)}$ , as well as hidden-charm production channels like  $\bar{p}p \rightarrow J/\psi X$ ,  $\eta_c\gamma$  [3, 4]. Corresponding theoretical studies have been performed within various frameworks, including the Jülich meson-baryon coupled-channel model [5, 6], effective Lagrangian and Regge frameworks [7–9], NRQCD factorization [10], and hadronic pole models [11, 12].

In parallel, J-PARC has developed complementary programs employing meson beams. The E50 spectrometer, for example, is designed to detect charged open-charm hadrons produced in  $\pi^-p \rightarrow D^{*-}Y_c^{*+}$  at an incident pion momentum of 20 GeV/c, where  $Y_c^{*+}$  denotes excited charmed baryons, such as  $\Lambda_c^*$ 's and  $\Sigma_c^*$ 's [13]. With its wide angular coverage and high momentum resolution, this experiment is expected to provide valuable information on charmed-baryon spectroscopy [14–16]. More recently, a new proposal (P111) has also been submitted to study hidden-charm production near threshold via  $\pi^-p \rightarrow J/\psi n$  [17]. Existing theoretical predictions for this cross section span orders of magnitude, ranging from  $\sigma_{\text{tot}} \sim 0.1$  pb [18] to  $\sim 50$  pb [19] and  $\sim 1.0$

nb [20] depending strongly on the assumed mechanism and model inputs. Reliable and model-constrained predictions are therefore essential for guiding experimental feasibility and optimizing detector design.

In previous works, the author and collaborators investigated open-strangeness ( $\pi^-p \rightarrow K^{(*)}\Lambda$ ) and open-charm ( $\pi^-p \rightarrow D^{(*)}\Lambda_c^+$ ) reactions [15, 21, 22] within a unified framework based on the quark-gluon string model (QGSM) [23–26]. In this picture, the annihilation of a  $q\bar{q}$  pair in the initial state leads to the formation of an intermediate string, which subsequently fragments into the observed hadrons via planar diagrams. A key advantage of the QGSM-based approach is that the two essential ingredients, Regge trajectories  $\alpha(t)$  and energy-scale parameters  $s_0$ , can be determined consistently across both the strangeness and charm sectors. Using the similarity of quark diagrams, hidden-strangeness ( $\pi^-p \rightarrow \phi n$ ) and hidden-charm ( $\pi^-p \rightarrow J/\psi n$ ) reactions were also studied in a coherent manner [18].

Beyond pion-induced reactions, J-PARC has established an extensive program of kaon-induced reactions using the high-intensity K1.8 beam line [2, 27, 28]. Motivated by these developments, in the present work, we extend the QGSM-motivated Regge framework [23–26] to kaon-induced reactions off the nucleon. We first analyze the strangeness production process  $K^-p \rightarrow \phi\Lambda$ , including both pseudoscalar  $K$ - and vector  $K^*$ -Reggeon exchanges in the  $t$  channel. We then provide predictions for the open-charm reaction  $K^-p \rightarrow D_s^{*-}\Lambda_c^+$  based on the same quark-level diagrammatic correspondence, where the parameters associated with  $D$ - and  $D^*$ -Reggeon exchanges are constrained within the QGSM framework. For the hidden-charm reaction  $K^-p \rightarrow J/\psi\Lambda$ , we employ the same  $K$ - and  $K^*$ -Reggeon exchange mechanisms but with appropriate coupling constants. All the cutoff

\* [shkimphy@gmail.com](mailto:shkimphy@gmail.com)

masses in the hadronic form factors are fixed by fitting the available  $K^- p \rightarrow \phi \Lambda$  data [29–31], thereby reducing model ambiguities and allowing more reliable predictions for charm production. We present results for the total cross sections,  $t$ -dependent differential cross sections, and spin-density matrix elements (SDMEs). In particular, SDMEs encode the helicity structure of the reaction amplitude and thus provide a stringent test of the underlying production mechanism [22].

The  $K^- p \rightarrow J/\psi \Lambda$  reaction is especially interesting because it offers direct access to possible hidden-charm pentaquark states with strangeness,  $P_{cs}$ , in the  $s$ -channel [32–34]. Recently, the LHCb Collaboration reported hidden-charm pentaquark candidates with quark content  $udsc\bar{c}$ . The  $P_{cs}(4459)^0$  state was observed in the analysis of the  $\Xi_b^- \rightarrow J/\psi \Lambda K^-$  decay [32], while the  $P_{cs}(4337)^0$  state was found in the  $B^- \rightarrow J/\psi \Lambda \bar{p}$  decay [34]. Their measured masses and widths are

$$\begin{aligned} M_{P_{cs}} &= 4458.8 \pm 2.9^{+4.7}_{-1.1}, \Gamma_{P_{cs}} = 17.3 \pm 6.5^{+8.0}_{-5.7} [32], \\ M_{P_{cs}} &= 4338.2 \pm 0.7 \pm 0.4, \Gamma_{P_{cs}} = 7.0 \pm 1.2 \pm 1.3 [34], \end{aligned} \quad (1)$$

respectively, in units of MeV. The dominant open-charm decay modes of these  $P_{cs}$  states have been studied theoretically within meson-baryon molecular pictures [35–46], some of which predict a sizable (possibly dominant) branching ratio into the  $D_s^* \Lambda_c$  channel [47, 48]. This suggests that the  $P_{cs}(4459)^0$  state may also be probed through the associated-production reaction  $K^- p \rightarrow D_s^{*-} \Lambda_c^+$ . Accordingly, we investigate possible  $s$ -channel contributions from the  $P_{cs}$  states to both the  $K^- p \rightarrow D_s^{*-} \Lambda_c^+$  and  $K^- p \rightarrow J/\psi \Lambda$  reactions.

This paper is organized as follows. In Sec. II, we present the formalism of the hybrid Regge approach and specify the model ingredients, including coupling constants, Regge trajectories, energy-scale parameters, and form factors. Section III contains numerical results for the total and differential cross sections as well as SDMEs, followed by discussion. Finally, Sec. IV summarizes our findings and provides concluding remarks.

## II. THEORETICAL FRAMEWORK

In this section, we introduce a hybrid Regge model that combines an effective Lagrangian approach with Regge phenomenology. As illustrated in Fig. 1, the strangeness reaction  $K^- p \rightarrow \phi \Lambda$  can be described by two quark diagrams. In Fig. 1(a), replacing the strange quark in the propagator with a charm quark ( $s \rightarrow c$ ) leads to the open-charm process  $K^- p \rightarrow D_s^{*-} \Lambda_c^+$ . In Fig. 1(b), the corresponding replacement in the produced vector meson results in the hidden-charm process  $K^- p \rightarrow J/\psi \Lambda$ .

For the  $K^- p \rightarrow \phi \Lambda$  and  $K^- p \rightarrow J/\psi \Lambda$  reactions, the  $t$ -channel contributions are described by pseudoscalar  $K$ - and vector  $K^*$ -Reggeon exchanges [Fig. 2(a)]. For

$K^- p \rightarrow D_s^{*-} \Lambda_c^+$ , we include pseudoscalar  $D$ - and vector  $D^*$ -Reggeon exchanges in the  $t$  channel [Fig. 2(b)].

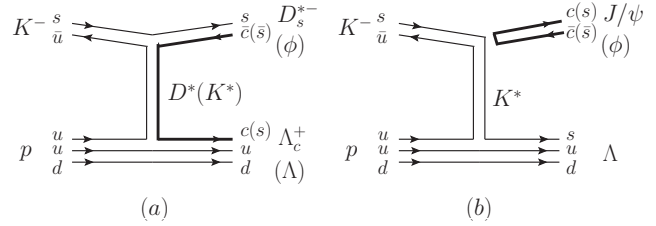


FIG. 1. Quark diagrams for (a)  $K^- p \rightarrow \phi \Lambda, D_s^{*-} \Lambda_c^+$  and (b)  $K^- p \rightarrow \phi \Lambda, J/\psi \Lambda$  in the  $t$  channel.

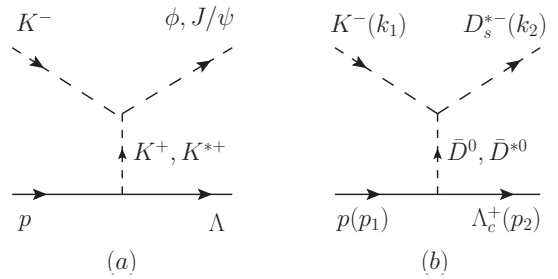


FIG. 2. Feynman diagrams for (a)  $t$ -channel  $K$ - and  $K^*$ -Reggeon exchanges for  $K^- p \rightarrow \phi \Lambda, J/\psi \Lambda$ , and (b)  $t$ -channel  $D$ - and  $D^*$ -Reggeon exchanges for  $K^- p \rightarrow D_s^{*-} \Lambda_c^+$ .

### A. Strangeness production: $K^- p \rightarrow \phi \Lambda$

We begin with the  $t$ -channel process of the  $K^- p \rightarrow \phi \Lambda$  reaction shown in Fig. 2. The four momenta of the initial  $K$  and proton are denoted by  $k_1$  and  $p_1$ , respectively, while those of the final  $\phi$  and  $\Lambda$  are denoted by  $k_2$  and  $p_2$ . The effective Lagrangians for the  $\phi KK$  and  $\phi K^* K$  vertices are given by

$$\begin{aligned} \mathcal{L}_{\phi KK} &= -ig_{\phi KK}(K^- \partial_\mu K^+ - \partial_\mu K^- K^+) \phi^\mu, \\ \mathcal{L}_{\phi K^* K} &= g_{\phi K^* K} \varepsilon^{\mu\nu\alpha\beta} \partial_\mu \phi_\nu (\partial_\alpha K_\beta^{*-} K^+ + \partial_\alpha K_\beta^{*+} K^-), \end{aligned} \quad (2)$$

where  $K$ , and  $K^*$ , and  $\phi$  represent the fields of  $K(494, 0^-)$ ,  $K^*(892, 1^-)$ , and  $\phi(1020, 1^-)$  mesons, respectively. The coupling constant  $g_{\phi KK} = 4.48$  is fixed from the branching ratio  $\mathcal{B}(\phi \rightarrow K^+ K^-) = 49.9\%$  [49] using the width of  $\Gamma_\phi = 4.249$  MeV and the relation,

$$\Gamma(\phi \rightarrow K^+ K^-) = \frac{p_K^3}{6\pi M_\phi^2} g_{\phi KK}^2, \quad (3)$$

where  $p_K = \sqrt{M_\phi^2 - 4M_K^2}/2$ . To obtain the coupling constant  $g_{\phi K^* K}$ , we use the SU(3) flavor symmetry relation,

$$g_{\phi K^* K} = g_{\rho \omega \pi} / \sqrt{2}, \quad (4)$$

where the coupling  $g_{\rho\omega\pi}$  is taken from the hidden gauge approach,

$$g_{\rho\omega\pi} = \frac{N_c g_{\phi\pi\pi}^2}{8\pi^2 f_\pi} = 14.4 \text{ GeV}^{-1}, \quad (5)$$

with  $N_c = 3$ ,  $f_\pi = 93$  MeV, and  $g_{\rho\pi\pi} = 5.94$  [50, 51].  $g_{\rho\pi\pi}$  is calculated from the branching ratio  $\mathcal{B}(\rho \rightarrow \pi\pi) \sim 1$  [49].

The effective Lagrangians for the meson-baryon octet vertices are written as

$$\begin{aligned} \mathcal{L}_{K N \Lambda} &= \frac{g_{K N \Lambda}}{M_N + M_\Lambda} \bar{N} \gamma_\mu \gamma_5 \Lambda \partial^\mu K + \text{H.c.}, \\ \mathcal{L}_{K^* N \Lambda} &= -g_{K^* N \Lambda} \bar{N} \left[ \gamma_\mu \Lambda - \frac{\kappa_{K^* N \Lambda}}{2M_N} \sigma_{\mu\nu} \Lambda \partial^\nu \right] K^{*\mu} + \text{H.c.}, \end{aligned} \quad (6)$$

where  $N$  and  $\Lambda$  stand for the nucleon and  $\Lambda(1116)$  baryon fields, respectively. The coupling constants are taken from the Nijmegen soft-core model (NSC97a) [52, 53],

$$\begin{aligned} g_{K N \Lambda} &= -13.4, \\ g_{K^* N \Lambda} &= -4.26, \quad \kappa_{K^* N \Lambda} = 2.66. \end{aligned} \quad (7)$$

The  $t$ -channel Regge amplitudes are constructed within a hybrid approach by replacing the Feynman propagators for pseudoscalar  $K$ - and vector  $K^*$ -meson exchanges with the corresponding Regge propagators associated with their Regge trajectories [7, 15],

$$\begin{aligned} T_K(s, t) &= \mathcal{M}_K(s, t) \left( \frac{s}{s_{K N: \phi \Lambda}} \right)^{\alpha_K(t)} \\ &\quad \times \Gamma(-\alpha_K(t)) \alpha'_K F_{PS}^2(t), \\ T_{K^*}(s, t) &= \mathcal{M}_{K^*}(s, t) \left( \frac{s}{s_{K^* N \Lambda}} \right)^{\alpha_{K^*}(t)-1} \\ &\quad \times \Gamma(1 - \alpha_{K^*}(t)) \alpha'_{K^*} F_V^2(t), \end{aligned} \quad (8)$$

where the amplitudes  $\mathcal{M}_K$  and  $\mathcal{M}_{K^*}$  are derived from the Lagrangians in Eq. (2), respectively,

$$\begin{aligned} \mathcal{M}_K^\mu &= 2i \frac{g_{\phi K K} g_{K N \Lambda}}{M_N + M_\Lambda} \gamma_\nu \gamma_5 k_1^\mu (k_2 - k_1)^\nu, \\ \mathcal{M}_{K^*}^\mu &= g_{\phi K^* K} g_{K^* N \Lambda} \epsilon^{\mu\nu\alpha\beta} \\ &\quad \times \left[ \gamma_\nu - \frac{i\kappa_{K^* N \Lambda}}{2M_N} \sigma_{\nu\lambda} (k_2 - k_1)^\lambda \right] k_{2\alpha} k_{1\beta}, \end{aligned} \quad (9)$$

with  $\mathcal{M} = \varepsilon_\mu^* \bar{u}_\Lambda \mathcal{M}^\mu u_N$ . Here  $u_N$  and  $u_\Lambda$  denote the Dirac spinors of the initial nucleon and the final  $\Lambda$ , respectively, and are normalized to  $\bar{u}_B u_B = 1$ . The four-vector  $\varepsilon_\mu$  stands for the polarization of the outgoing  $\phi$  meson.

The form factor in Eq. (8) is introduced to dress the vertices in the diagrams. We adopt the following form:

$$F_{PS(V)}(t) = \frac{\Lambda_{PS(V)}^2}{\Lambda_{PS(V)}^2 - t}. \quad (10)$$

The differential cross section  $d\sigma/dt$  is expressed as

$$\frac{d\sigma}{dt} = \frac{M_N M_\Lambda}{16\pi(p_{\text{c.m.}})^2 s} \frac{1}{2} \sum_{\lambda_V, s_f, s_i} |T|^2, \quad (11)$$

where  $p_{\text{c.m.}}$  denotes the kaon momentum in the center-of-mass (c.m.) frame.  $s_i$ ,  $s_f$ , and  $\lambda_V$  label the helicity states of the nucleon, the  $\Lambda$  baryon, and the  $\phi$  meson, respectively.

$d\sigma/dt$  satisfies the following asymptotic behavior:

$$\frac{d\sigma}{dt}(s \rightarrow \infty, t \rightarrow 0) \propto s^{2\alpha(0)-2}. \quad (12)$$

More specifically, the asymptotic behaviors of the squared amplitudes of Eq. (9) are derived as

$$\begin{aligned} \lim_{s \rightarrow \infty} \sum_{\lambda_V, s_f, s_i} |\mathcal{M}_K(s, t)|^2 &\propto A, \\ \lim_{s \rightarrow \infty} \sum_{\lambda_V, s_f, s_i} |\mathcal{M}_{K^*}(s, t)|^2 &\propto -Bs^2 t + Cs^2 t^2, \end{aligned} \quad (13)$$

where  $A$ ,  $B$ , and  $C$  are kinematics-independent constants, leading to distinct cross-section shapes at very forward angles. For  $K$ -Reggeon exchange, the cross section increases monotonically in this region, whereas for  $K^*$ -Reggeon exchange the presence of an antisymmetric tensor in the amplitude substantially reduces the cross section at very forward angles.

To determine the  $K$ -and  $K^*$ -Regge trajectories in Eq. (8), we follow Ref. [54], where the so-called “square-root” trajectory is adopted,

$$\alpha(t) = \alpha(0) + \gamma [\sqrt{T} - \sqrt{T-t}], \quad (14)$$

with  $\gamma$  the universal slope and  $T$  a scale parameter specific to each trajectory. In the limit  $-t \ll T$ , Eq. (14) can be approximated by a linear form,

$$\alpha(t) = \alpha(0) + \alpha' t, \quad (15)$$

with the slope  $\alpha' = \gamma/(2\sqrt{T})$ . In Ref. [54], the parameters  $\sqrt{T}$  for the  $\pi$ - and  $\rho$ -Regge trajectories were determined as

$$\begin{aligned} \sqrt{T_\pi} &= 2.82 \pm 0.05 \text{ GeV}, \\ \sqrt{T_\rho} &= 2.46 \pm 0.03 \text{ GeV}, \end{aligned} \quad (16)$$

with  $\gamma = 3.65 \pm 0.05 \text{ GeV}^{-1}$ . Following the same procedure, we extract the corresponding values of  $\sqrt{T}$  for the  $K$ - and  $K^*$ -Regge trajectories.

The  $\eta_s$ - and  $\phi$ -Regge trajectories are determined using the additivity relations of the intercepts and inverse slopes,

$$\begin{aligned} 2\alpha_{\bar{s}q}(0) &= \alpha_{\bar{q}q}(0) + \alpha_{\bar{s}s}(0), \\ 2/\alpha'_{\bar{s}q} &= 1/\alpha'_{\bar{q}q} + 1/\alpha'_{\bar{s}s}, \end{aligned} \quad (17)$$

	$\alpha(0)$	$\sqrt{T}$ [GeV]	$\alpha'$ [GeV $^{-2}$ ]
$\bar{q}q(\pi)$	-0.0118	2.82	0.647
$\bar{s}q(K)$	-0.151	2.96	0.617
$\bar{s}s(\eta_s)$	-0.291	3.10	0.589
$\bar{q}q(\rho)$	0.55	2.46	0.742
$\bar{s}q(K^*)$	0.414	2.58	0.707
$\bar{s}s(\phi)$	0.27	2.70	0.676

TABLE I. The pseudoscalar- and vector-meson trajectories in the strange sector [7, 54].

where the  $\alpha_{\bar{q}q}(t)$ ,  $\alpha_{\bar{s}q}(t)$ , and  $\alpha_{\bar{s}s}(t)$  denote the trajectories corresponding to  $\pi$ ,  $K$ , and  $\eta_s$  for pseudoscalar mesons, and to  $\rho$ ,  $K^*$ , and  $\phi$  for vector mesons, respectively. All Regge-trajectory parameters are summarized in Table I.

With the Regge trajectories determined, the energy-scale parameters  $s_K^{KN:\phi\Lambda}$  and  $s_{K^*}^{KN:\phi\Lambda}$  in Eq. (8) can be derived using the corresponding scale parameters for the diagonal transitions  $KN \rightarrow KN(s^{KN})$  and  $\phi\Lambda \rightarrow \phi\Lambda(s^{\phi\Lambda})$  as [24–26]

$$(s_K^{KN:\phi\Lambda})^{2(\alpha_K(0))} = (s^{KN})^{\alpha_\pi(0)} \times (s^{\phi\Lambda})^{\alpha_{\eta_s}(0)} \\ (s_{K^*}^{KN:\phi\Lambda})^{2(\alpha_{K^*}(0)-1)} = (s^{KN})^{\alpha_\rho(0)-1} \times (s^{\phi\Lambda})^{\alpha_\phi(0)-1} \quad (18)$$

where  $s^{ab}$  is proportional to the total transverse masses of the constituent quarks in hadrons  $a$  and  $b$ ,

$$s^{ab} = \left( \sum_i m_{\perp i} \right)_a \left( \sum_j m_{\perp j} \right)_b. \quad (19)$$

We use  $m_{\perp q} \simeq 0.5$  GeV,  $m_{\perp s} \simeq 0.6$  GeV, and  $m_{\perp c} \simeq 1.6$  GeV, which lead to

$$s^{KN} = 1.65, \quad s^{\phi\Lambda} = 1.92, \\ s_K^{KN:\phi\Lambda} = 1.91, \quad s_{K^*}^{KN:\phi\Lambda} = 1.82, \quad (20)$$

in units of GeV $^2$ .

### B. Charm production: $K^- p \rightarrow D_s^{*-} \Lambda_c^+, J/\psi \Lambda$

We extend the analysis of strangeness production in  $K^- p \rightarrow \phi\Lambda$  to charm production by simply replacing strange hadrons with charm hadrons.

#### 1. $K^- p \rightarrow D_s^{*-} \Lambda_c^+$

The  $t$ -channel Regge amplitudes for the  $K^- p \rightarrow D_s^{*-} \Lambda_c^+$  reaction are obtained by replacing  $K \rightarrow D(1869, 0^-)$  and  $K^* \rightarrow D^*(2007, 1^-)$  in the propagators, and  $\phi \rightarrow D_s^*(2106, 1^-)$  and  $\Lambda \rightarrow \Lambda_c(2286, 1/2^+)$  in the

final states (Fig 1(a)):

$$T_D(s, t) = \mathcal{M}_D(s, t) \left( \frac{s}{s_D^{KN:D_s^*\Lambda_c}} \right)^{\alpha_D(t)} \\ \times \Gamma(-\alpha_D(t)) \alpha'_D F_{PS}^2(t), \\ T_{D^*}(s, t) = \mathcal{M}_{D^*}(s, t) \left( \frac{s}{s_{D^*}^{KN:D_s^*\Lambda_c}} \right)^{\alpha_{D^*}(t)-1} \\ \times \Gamma(1 - \alpha_{D^*}(t)) \alpha'_{D^*} F_V^2(t). \quad (21)$$

The  $D$ - and  $D^*$ -Regge trajectories are determined as in the strangeness production case. The relevant values are listed in Table II [54].

	$\alpha(0)$	$\sqrt{T}$ [GeV]	$\alpha'$ [GeV $^{-2}$ ]
$\bar{q}q(\pi)$	-0.0118	2.82	0.647
$\bar{c}q(D)$	-1.61105	4.16	0.439
$\bar{c}c(\eta_c)$	-3.2103	5.49	0.332
$\bar{q}q(\rho)$	0.55	2.46	0.742
$\bar{c}q(D^*)$	-1.02	3.91	0.467
$\bar{c}c(J/\psi)$	-2.60	5.36	0.340

TABLE II. Pseudoscalar- and vector-meson trajectories in the charm sector [54].

Equation (18) can be also modified as [24–26]

$$(s_D^{KN:D_s^*\Lambda_c})^{2\alpha_D(0)} = (s^{KN})^{\alpha_\pi(0)} \times (s^{D_s^*\Lambda_c})^{\alpha_{\eta_c}(0)} \\ (s_{D^*}^{KN:D_s^*\Lambda_c})^{2(\alpha_{D^*}(0)-1)} = (s^{KN})^{\alpha_\rho(0)-1} \times (s^{D_s^*\Lambda_c})^{\alpha_{J/\psi}(0)-1}, \quad (22)$$

where

$$s^{KN} = 1.65, \quad s^{D_s^*\Lambda_c} = 5.72, \\ s_D^{KN:D_s^*\Lambda_c} = 5.69, \quad s_{D^*}^{KN:D_s^*\Lambda_c} = 5.00, \quad (23)$$

in units of GeV $^2$ .

The coupling constants in Eq. (9) are replaced as  $g_{\phi KK} \rightarrow g_{D_s^* D K}$  and  $g_{\phi K^* K} \rightarrow g_{D_s^* D^* K}$ . The coupling  $g_{D_s^* D K}$  is fixed using SU(4) flavor symmetry as  $g_{D_s^* D K} = g_{\rho\pi\pi}/\sqrt{2}$  [5], where  $g_{\rho\pi\pi} = 5.94$ . The strength of the  $D_s^* D^* K$  vertex is then estimated from heavy-quark spin symmetry, which relates it to  $g_{D_s^* D K}$  through  $g_{D_s^* D^* K} = -g_{D_s^* D K}/\sqrt{M_D M_{D^*}} = -1.53$  GeV $^{-1}$  [55, 56]. For the meson–baryon couplings, we assume SU(4) symmetry and take them to be identical to those in the strange sector, namely  $g_{D N \Lambda_c} = g_{K N \Lambda}$ ,  $g_{D^* N \Lambda_c} = g_{K^* N \Lambda}$ , and  $\kappa_{D^* N \Lambda_c} = \kappa_{K^* N \Lambda}$ . In the tensor term, the same mass scale  $M_N$  as in the strange sector is employed.

#### 2. $K^- p \rightarrow J/\psi \Lambda$

The  $t$ -channel Regge amplitudes for the  $K^- p \rightarrow J/\psi \Lambda$  reaction are obtained just by replacing  $\phi \rightarrow$

$J/\psi(3096, 1^-)$  in the final state (Fig 1(b)):

$$\begin{aligned} T_K(s, t) &= \mathcal{M}_K(s, t) \left( \frac{s}{s_K^{KN:J/\psi\Lambda}} \right)^{\alpha_K(t)} \\ &\times \Gamma(-\alpha_K(t)) \alpha'_K F_{PS}^2(t), \\ T_{K^*}(s, t) &= \mathcal{M}_{K^*}(s, t) \left( \frac{s}{s_{K^*}^{KN:J/\psi\Lambda}} \right)^{\alpha_{K^*}(t)-1} \\ &\times \Gamma(1 - \alpha_{K^*}(t)) \alpha'_{K^*} F_V^2(t). \end{aligned} \quad (24)$$

The energy scale parameters are assumed to be the same as those in the strange sector:  $s_K^{KN:J/\psi\Lambda} = s_K^{KN:\phi\Lambda}$  and  $s_{K^*}^{KN:J/\psi\Lambda} = s_{K^*}^{KN:\phi\Lambda}$ .

The coupling constants in Eq. (9) are replaced as  $g_{\phi KK} \rightarrow g_{J/\psi KK}$  and  $g_{\phi K^* K} \rightarrow g_{J/\psi K^* K}$ . Since the branching ratios of  $J/\psi$  to the  $K$  and  $K^*$  are known experimentally as

$$\begin{aligned} \mathcal{B}(J/\psi \rightarrow K^+ K^-) &= 0.0306\%, \\ \mathcal{B}(J/\psi \rightarrow K^+ K^{*-}) &= 0.60\%, \end{aligned} \quad (25)$$

we can get their coupling constants as

$$\begin{aligned} g_{J/\psi KK} &= 1.28 \cdot 10^{-3}, \\ g_{J/\psi K^* K} &= 2.85 \cdot 10^{-3} \text{ GeV}^{-1}, \end{aligned} \quad (26)$$

using the width of  $\Gamma_{J/\psi} = 92.6$  keV and the relations,

$$\begin{aligned} \Gamma(J/\psi \rightarrow K^+ K^-) &= \frac{q_K^3}{6\pi M_{J/\psi}^2} g_{J/\psi KK}^2, \\ \Gamma(J/\psi \rightarrow K^+ K^{*-}) &= \frac{q_{K^*}^3}{12\pi} g_{J/\psi K^* K}^2, \end{aligned} \quad (27)$$

where  $q_{K(K^*)}$  is the magnitude of the three-momentum of  $K(K^*)$  in the rest frame of  $J/\psi$ .

### C. $s$ - and $u$ -channel contributions to $K^- p \rightarrow \phi\Lambda$

The  $s$ -channel  $\Lambda$  [Fig. 3(a)] and  $u$ -channel nucleon [Fig. 3(b)] exchanges may contribute to the  $K^- p \rightarrow \phi\Lambda$  reaction, and they are examined in this work.

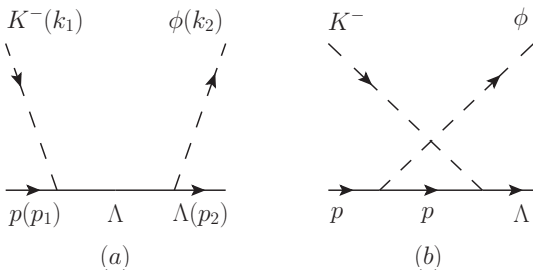


FIG. 3. Feynman diagrams for  $K^- p \rightarrow \phi\Lambda$ : (a)  $\Lambda$  exchange in the  $s$  channel and (b) nucleon exchange in the  $u$  channel.

The effective Lagrangians for the  $\phi$ -meson–baryon interaction vertices are written as

$$\begin{aligned} \mathcal{L}_{\phi\Lambda\Lambda} &= -g_{\phi\Lambda\Lambda}\bar{\Lambda} \left[ \gamma_\mu\Lambda - \frac{\kappa_{\phi\Lambda\Lambda}}{2M_N}\sigma_{\mu\nu}\Lambda\partial^\nu \right] \phi^\mu, \\ \mathcal{L}_{\phi NN} &= -g_{\phi NN}\bar{N} \left[ \gamma_\mu N - \frac{\kappa_{\phi NN}}{2M_N}\sigma_{\mu\nu}N\partial^\nu \right] \phi^\mu, \end{aligned} \quad (28)$$

where the Nijmegen soft-core model (NSC97a) [52, 53] is used to determine the coupling constants,

$$\begin{aligned} g_{\phi\Lambda\Lambda} &= -3.80, \quad \kappa_{\phi\Lambda\Lambda} = 1.78, \\ g_{\phi NN} &= -1.47, \quad \kappa_{\phi NN} = -2.64. \end{aligned} \quad (29)$$

The scattering amplitudes corresponding to the  $s$ -channel  $\Lambda$  and  $u$ -channel nucleon exchanges are, respectively, given by

$$\begin{aligned} \mathcal{M}_\Lambda^\mu &= i \frac{g_{\phi\Lambda\Lambda}}{s - M_\Lambda^2} \frac{g_{K\Lambda}}{M_N + M_\Lambda} \left[ \gamma^\mu - \frac{i\kappa_{\phi\Lambda\Lambda}}{2M_N}\sigma^{\mu\nu}k_{2\nu} \right] \\ &\times (\not{k}_1 + \not{p}_1 + M_\Lambda)\gamma^\alpha\gamma_5k_{1\alpha}, \\ \mathcal{M}_N^\mu &= i \frac{g_{\phi NN}}{u - M_N^2} \frac{g_{K\Lambda}}{M_N + M_\Lambda} \gamma^\alpha\gamma_5(\not{p}_2 - \not{k}_1 + M_N) \\ &\times \left[ \gamma^\mu - \frac{i\kappa_{\phi NN}}{2M_N}\sigma^{\mu\nu}k_{2\nu} \right] k_{1\alpha}. \end{aligned} \quad (30)$$

with  $\mathcal{M} = \varepsilon_\mu^* \bar{u}_\Lambda \mathcal{M}^\mu u_N$ . The relevant hadrons are spatially extended, so we consider the following form factor for each vertex:

$$\begin{aligned} F_\Lambda(s) &= \frac{\Lambda_s^4}{\Lambda_s^4 + (s - M_\Lambda^2)^2}, \\ F_N(u) &= \frac{\Lambda_u^4}{\Lambda_u^4 + (u - M_N^2)^2}, \end{aligned} \quad (31)$$

for the  $s$ -channel and  $u$ -channel diagrams, respectively. The cutoff masses are determined to be  $\Lambda_s = \Lambda_u = 0.8$  GeV.

### D. Pentaquark contributions to $K^- p \rightarrow D_s^{*-} \Lambda_c^+, J/\psi\Lambda$

We now examine the  $s$ -channel contributions from the hidden-charm pentaquark states with strangeness,  $P_{cs}(4337)^0$  [34] and  $P_{cs}(4459)^0$  [32], as shown in Fig. 4. We point out that  $P_{cs}(4337)^0$  exchange is allowed only for  $K^- p \rightarrow J/\psi\Lambda$ , because the  $D_s^{*-} \Lambda_c^+$  production threshold lies above the  $P_{cs}(4337)^0$  mass.

While the spin-parity of  $P_{cs}(4337)^0$  has been determined to be  $J^P = 1/2^-$ , that of  $P_{cs}(4459)^0$  is still unsettled. In a hadronic molecular interpretation, Ref. [36] favors  $J^P = 3/2^-$  over  $1/2^-$ , which is also supported by Ref. [47]. In contrast, within a unitarized approach,  $J^P = 1/2^-$  is preferred over  $3/2^-$  [57]. Accordingly, we consider both  $J^P = 1/2^-$  and  $3/2^-$  assignments for

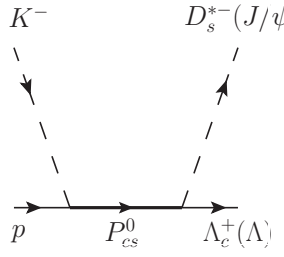


FIG. 4. Feynman diagram for the  $K^- p \rightarrow D_s^{*-} \Lambda_c^+$ ,  $J/\psi \Lambda$  reactions via  $s$ -channel  $P_{cs}^0$  pentaquark exchange.

$P_{cs}(4459)^0$  in our analysis. The branching ratios are taken as follows [48]:

$$\begin{aligned} \mathcal{B}(P_{cs}(4459, 1/2^-) \rightarrow \bar{D}_s^* \Lambda_c) &= 80.86\%, \\ \mathcal{B}(P_{cs}(4459, 3/2^-) \rightarrow \bar{D}_s^* \Lambda_c) &= 81.64\%, \\ \mathcal{B}(P_{cs}(4459, 1/2^-) \rightarrow J/\psi \Lambda) &= 3.31\%, \\ \mathcal{B}(P_{cs}(4459, 3/2^-) \rightarrow J/\psi \Lambda) &= 14.68\%. \end{aligned} \quad (32)$$

For  $P_{cs}(4337)^0$ , we adopt the branching ratio quoted in Ref. [58],

$$\mathcal{B}(P_{cs}(4337) \rightarrow J/\psi \Lambda) = 84.7\%. \quad (33)$$

Note that since no information is currently available for the  $P_{cs} \rightarrow \bar{K}N$  branching ratios of  $P_{cs}(4337)^0$  and  $P_{cs}(4459)^0$ , we treat them as free parameters in the present analysis.

The effective Lagrangians for the  $P_{cs}NK$  vertex are given by [59]

$$\begin{aligned} \mathcal{L}_{PNK}^{1/2^\pm} &= -ig_{PNK} \bar{N} \Gamma^{(\pm)} P K + \text{H.c.}, \\ \mathcal{L}_{PNK}^{3/2^\pm} &= \frac{g_{PNK}}{M_K} \bar{N} \Gamma^{(\mp)} P^\mu \partial_\mu K + \text{H.c.}, \end{aligned} \quad (34)$$

where the off-shell part of the Rarita-Schwinger fields is also ignored because the resonances are almost on mass shell. For the  $K^- p \rightarrow D_s^{*-} \Lambda_c^+$  reaction, the effective Lagrangians for the  $P_{cs} \Lambda_c D_s^*$  vertex can be expressed as [59]

$$\begin{aligned} \mathcal{L}_{P\Lambda_c D_s^*}^{1/2^\pm} &= -g_{P\Lambda_c D_s^*} \bar{\Lambda}_c \Gamma_\mu^{(\mp)} P D_s^{*\mu} + \text{H.c.}, \\ \mathcal{L}_{P\Lambda_c D_s^*}^{3/2^\pm} &= -\frac{ig_{P\Lambda_c D_s^*}}{2M_N} \bar{\Lambda}_c \Gamma_\nu^{(\pm)} P_\mu D_s^{*\mu\nu} + \text{H.c.}, \end{aligned} \quad (35)$$

where  $D_s^{*\mu\nu} = \partial^\mu D_s^{*\nu} - \partial^\nu D_s^{*\mu}$ . The heavy pentaquark states play a dominant role near the threshold region, so additional terms are ignored.  $P$  denotes the field of the pentaquark state  $P_{cs}$ . For the  $K^- p \rightarrow J/\psi \Lambda$  reaction, we can just replace the hadrons as  $D_s^* \rightarrow J/\psi$  and  $\Lambda_c \rightarrow \Lambda$ .

The following notations are used:

$$\Gamma^{(\pm)} = \begin{pmatrix} \gamma_5 \\ \mathbf{1} \end{pmatrix}, \quad \Gamma_\mu^{(\pm)} = \begin{pmatrix} \gamma_\mu \gamma_5 \\ \gamma_\mu \end{pmatrix}. \quad (36)$$

The scattering amplitudes for the exchanges of the pentaquark states are written as

$$\begin{aligned} \mathcal{M}_{P(1/2^+)}^\mu &= i \frac{g_{PNK} g_{P\Lambda_c D_s^*}}{s - M_P^2} \gamma^\mu (\not{q}_s + M_P) \gamma_5, \\ \mathcal{M}_{P(1/2^-)}^\mu &= i \frac{g_{PNK} g_{P\Lambda_c D_s^*}}{s - M_P^2} \gamma^\mu \gamma_5 (\not{q}_s + M_P), \\ \mathcal{M}_{P(3/2^+)}^\mu &= i \frac{g_{PNK}}{M_K} \frac{g_{P\Lambda_c D_s^*}}{2M_N} \frac{1}{s - M_P^2} \gamma_5 \gamma_\nu \\ &\quad \times (k_1^\alpha g^{\mu\nu} - k_2^\nu g^{\mu\alpha}) \Delta_{\alpha\beta}(q_s, M_P) k_1^\beta, \\ \mathcal{M}_{P(3/2^-)}^\mu &= i \frac{g_{PNK}}{M_K} \frac{g_{P\Lambda_c D_s^*}}{2M_N} \frac{1}{s - M_P^2} \gamma_\nu \\ &\quad \times (k_2^\alpha g^{\mu\nu} - k_2^\nu g^{\mu\alpha}) \Delta_{\alpha\beta}(q_s, M_P) k_1^\beta \gamma_5, \end{aligned} \quad (37)$$

with  $\mathcal{M} = \varepsilon_\mu^* \bar{u}_\Lambda \mathcal{M}^\mu u_N$  and  $q_s = k_1 + p_1$ . The spin-3/2 projection operator is given by

$$\begin{aligned} \Delta_{\alpha\beta}(p, M) &= (\not{p} + M) \left[ -g_{\alpha\beta} + \frac{1}{3} \gamma_\alpha \gamma_\beta \right. \\ &\quad \left. + \frac{1}{3M} (\gamma_\alpha p_\beta - p_\alpha \gamma_\beta) + \frac{2}{3M^2} p_\alpha p_\beta \right] \end{aligned} \quad (38)$$

Given the decay widths of the  $P_{cs}$  states, the propagators of the pentaquark states should be modified to  $M_{P_{cs}} \rightarrow (M_{P_{cs}} - i\Gamma_{P_{cs}}/2)$ .

From the values of branching ratios given in Eqs. (32) and (33), the coupling constants for the  $P_{cs}$  interactions are obtained and are summarized in Table III [59].

	$g_{P\Lambda_c D_s^*}$	$g_{P\Lambda J/\psi}$
$P_{cs}(4459, 1/2^-)$	0.382	0.0802
$P_{cs}(4459, 3/2^-)$	0.589	0.176
$P_{cs}(4380)$	—	0.313

TABLE III. Coupling constants of  $P_{cs}(4459)$  to  $D_s^* \Lambda_c$  and  $J/\psi \Lambda$  for each  $J^P = 1/2^-$  and  $3/2^-$  assignment, together with that of  $P_{cs}(4380)$  to  $J/\psi \Lambda$ .

We consider the form factor

$$F_{P_{cs}}(s) = \frac{\Lambda_P^4}{\Lambda_P^4 + (s - M_{P_{cs}}^2)^2}, \quad (39)$$

at each vertex, where the cutoff masses are selected as  $\Lambda_P = 1.0$  GeV. This cutoff mass does not play a crucial role in the present calculation, since the  $P_{cs}$  states lie close to the reaction threshold.

## E. Spin density matrix elements

The SDMEs, which characterize the polarization states of the relevant hadrons, provide key observables for understanding the reaction mechanism [22]. In this work, we focus on the case in which only the produced vector meson is polarized. For definiteness, we consider the

decay channel  $\phi \rightarrow K^+ K^-$  in the  $K^- p \rightarrow \phi \Lambda$  reaction. The analysis of the outgoing  $K^+$  in the vector-meson rest frame involves an ambiguity in the choice of the quantization axis. One possible choice is to take the axis antiparallel to the momentum of the outgoing hyperon  $\Lambda$  in the  $\phi$  decay. Alternatively, it may be defined to be parallel to the momentum of the incoming meson, i.e., along the initial beam direction.

Following the convention of Refs. [60, 61], the former choice is referred to as the helicity (H) frame, while the latter is known as the Gottfried–Jackson (GJ) frame. The helicity frame is commonly used to test  $s$ -channel helicity conservation, whereas the GJ frame is suitable for investigating the  $t$ -channel exchange mechanism.

The decay probabilities are expressed in terms of the spin density matrix elements  $\rho_{\lambda\lambda'}$ , where the vector-meson helicity  $\lambda_V$  is abbreviated as  $\lambda$ . These SDMEs are determined by the reaction amplitudes given by Eq. (8)

$$\rho_{\lambda\lambda'} = \frac{1}{\mathcal{N}^2} \sum_{s_f=\pm\frac{1}{2}, s_i=\pm\frac{1}{2}} T_{\lambda, s_f; s_i} T_{\lambda', s_f; s_i}^*, \quad (40)$$

with the normalization factor

$$\mathcal{N}^2 = \sum_{\lambda, s_f, s_i} |T_{\lambda, s_f; s_i}|^2. \quad (41)$$

We make use of the Hermitian conditions,

$$\rho_{1-1} = \rho_{-11}, \quad \rho_{10} = \rho_{01}, \quad \rho_{-10} = \rho_{0-1}. \quad (42)$$

In addition, the normalization condition  $\rho_{00} + \rho_{11} + \rho_{-1-1} = 1$  and the symmetry conditions,

$$\begin{aligned} \rho_{11} &= \rho_{-1-1}, \quad \rho_{\pm 10} = \rho_{0\pm 1}, \\ \rho_{1-1} &= \rho_{-11}, \quad \rho_{\pm 10} = -\rho_{0\mp 1}, \end{aligned} \quad (43)$$

are satisfied in our numerical calculations.

The decay angular distributions can be expressed in terms of the SDMEs as

$$\begin{aligned} W^0(\Omega_f) &= \frac{3}{4\pi} \left[ \rho_{00} \cos^2 \Theta + \rho_{11} \sin^2 \Theta - \rho_{1-1} \sin^2 \Theta \cos 2\Phi \right. \\ &\quad \left. - \sqrt{2} \operatorname{Re}(\rho_{10}) \sin 2\Theta \cos \Phi \right], \end{aligned} \quad (44)$$

denoting the polar and the azimuthal angles of the outgoing pseudoscalar  $K^+$  meson by  $\Theta$  and  $\Phi$ , respectively [22].

### III. NUMERICAL RESULTS

#### A. Strangeness production: $K^- p \rightarrow \phi \Lambda$

We first present our numerical results for the  $K^- p \rightarrow \phi \Lambda$  reaction, considering the  $K$ - and  $K^*$ -Reggeon exchanges discussed in Sec. II A. The cutoff masses in the

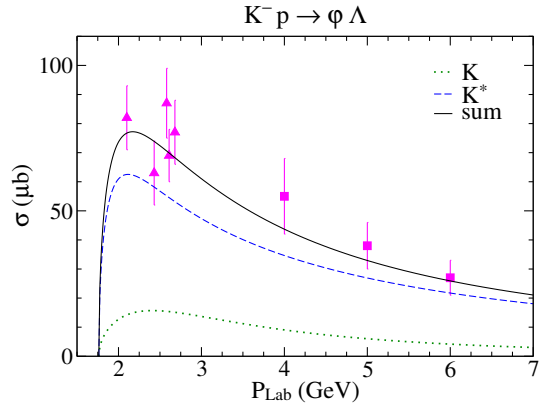


FIG. 5. Total cross section for the  $K^- p \rightarrow \phi \Lambda$  reaction as a function of  $P_{\text{Lab}}$ . The green dotted and blue dashed curves denote the contributions from  $K$ - and  $K^*$ -Reggeon exchanges, respectively, while the black solid curve represents their sum. Experimental data are taken from Ref. [29] (triangles) and [30] (squares).

form factor of Eq. (10) are fixed by reproducing the available data,

$$\Lambda_{PS} = 0.5 \text{ GeV}, \quad \Lambda_V = 0.8 \text{ GeV}. \quad (45)$$

Figure 5 displays the total cross section as a function of the laboratory beam energy,  $P_{\text{Lab}}$ . The  $K^*$ -Reggeon exchange clearly dominates over the  $K$ -Reggeon exchange, and its contribution becomes increasingly important at higher beam energies. The coherent sum of the two exchanges provides a good overall description of the experimental data [29, 30].

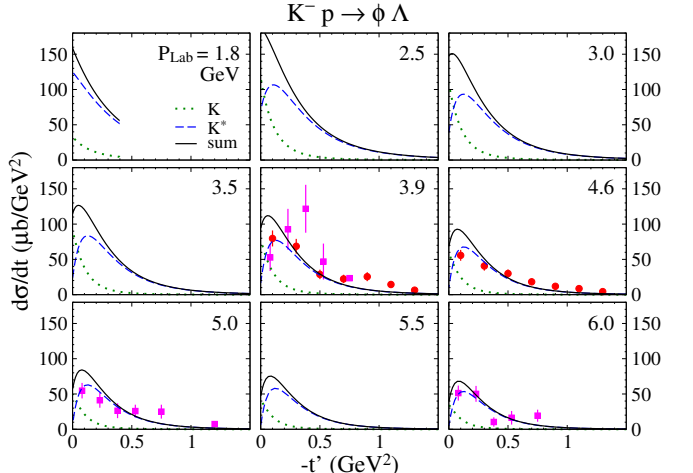


FIG. 6.  $t$ -dependent differential cross sections for the  $K^- p \rightarrow \phi \Lambda$  reaction at nine fixed beam energies. Experimental data are taken from Refs. [31] (circles) and [30] (squares). Curve notations are the same as in Fig. 5.

We present the differential cross sections as functions of  $-t' = -t + t_{\min}$  in Fig. 6 at nine fixed beam energies. As discussed in Eq. (13), the two Reggeon exchanges ex-

hibit qualitatively different behaviors at very forward angles. The available experimental data strongly favor the  $K^*$ -Reggeon exchange over the  $K$ -Reggeon exchange. A larger  $K$ -Reggeon contribution would worsen the agreement [30, 31].

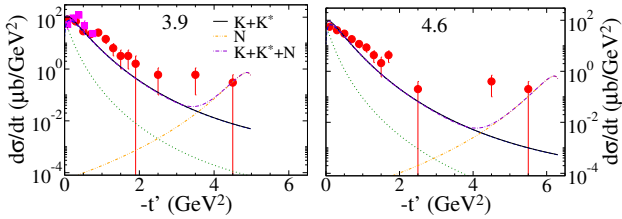


FIG. 7.  $t$ -dependent differential cross sections for the  $K^- p \rightarrow \phi\Lambda$  reaction at  $P_{\text{Lab}} = 3.9$  and  $4.6$  GeV, shown on a logarithmic scale. Experimental data are taken from Refs. [31] (circles) and [30] (squares). In addition to  $t$ -channel  $K$ - and  $K^*$ -Reggeon exchanges,  $u$ -channel nucleon exchange is also included.

In Fig. 7, we examine additional contributions from the  $s$ -channel  $\Lambda$  and  $u$ -channel nucleon exchanges, taking advantage of the backward-angle scattering data reported in Ref. [31]. The  $K^*$ -Reggeon exchange reproduces the slope of the experimental data well, which supports the validity of our Regge formalism. Owing to the different intercepts of the Regge trajectories,  $\alpha_K(0) < \alpha_{K^*}(0)$ , the  $K$ -Reggeon exchange decreases more rapidly with increasing  $-t'$  than the  $K^*$ -Reggeon exchange, as indicated in Eq. (12). The small deviations observed at  $-t' \geq 4 \text{ GeV}^2$  can be accounted for by including the  $u$ -channel nucleon contribution. In contrast, the  $s$ -channel  $\Lambda$  exchange interferes destructively with the  $t$ -channel contribution at backward angles and is therefore strongly suppressed in this mechanism.

The role of the individual contributions becomes evident in Fig. 8, where the SDMEs are shown as functions of  $-t'$  at  $P_{\text{Lab}} = 4.2$  and  $5$  GeV in both the helicity and GJ frames [22]. In general, including the  $K$ -Reggeon exchange in addition to the  $K^*$  Reggeon contribution improves the overall description of the SDMEs. In particular, the  $t$  dependences of  $\rho_{00}^H$  and  $\text{Re} \rho_{10}^H$  from the  $K$ -Reggeon exchange closely follow those of the corresponding experimental data.

### B. Charm production: $K^- p \rightarrow D_s^{*-} \Lambda_c^+$ , $J/\psi\Lambda$

We now turn to charm production described in Sec. II B and compare the results with those for the strangeness production  $K^- p \rightarrow \phi\Lambda$ . Figure 9 depicts the predicted total cross sections for the  $K^- p \rightarrow D_s^{*-} \Lambda_c^+$  and  $K^- p \rightarrow J/\psi\Lambda$  reactions as functions of  $P_{\text{Lab}}$ . In both cases, vector-meson Reggeon exchanges dominate, similarly to the strangeness production channel. Owing to the much larger mass gap in the final state of the  $K^- p \rightarrow J/\psi\Lambda$  channel, its total cross section increases more gradually with  $P_{\text{Lab}}$  than those of the  $K^- p \rightarrow \phi\Lambda$

and  $K^- p \rightarrow D_s^{*-} \Lambda_c^+$  reactions. Our result for  $K^- p \rightarrow J/\psi\Lambda$  is approximately three orders of magnitude smaller than that predicted in Ref. [62].

A direct comparison among the  $\phi\Lambda$ ,  $D_s^{*-} \Lambda_c^+$ , and  $J/\psi\Lambda$  production is given in Fig. 10(a) as functions of  $s/s_{\text{th}}$ , where  $s_{\text{th}}$  is the threshold energy of the corresponding reaction. The total cross section for the open-charm reaction  $K^- p \rightarrow D_s^{*-} \Lambda_c^+$  is suppressed by approximately 5-6 orders of magnitude compared with that for the strangeness reaction  $K^- p \rightarrow \phi\Lambda$  depending on the kinematical region. This suppression can be attributed mainly to the larger energy-scale parameter in the charm sector,  $s_{D(D^*)}^{KN:D_s^{*-} \Lambda_c^+} > s_{K(K^*)}^{KN:\phi\Lambda}$ , as well as to the smaller coupling strength,  $g_{D_s^{*} D^* K} < g_{\phi K^* K}$ . In the case of the hidden-charm reaction  $K^- p \rightarrow J/\psi\Lambda$ , the total cross section is further suppressed by about 8-9 orders of magnitude compared to that for the strangeness reaction  $K^- p \rightarrow \phi\Lambda$ , even though the same Regge parameters are employed. This stronger suppression mainly arises from the much smaller coupling strength in the charm sector,  $g_{\phi K^* K} \simeq 3.5 \cdot 10^3 g_{J/\psi K^* K}$ .

It is worthwhile to compare the results shown in Fig. 10(a) with those of the relevant pion-induced reactions studied in Refs. [15, 18] within a similar theoretical framework. In Fig. 10(b), we compare the total cross sections for the reactions  $\pi^- p \rightarrow K^{*0} \Lambda$  [61, 63],  $\phi n$  [30, 64],  $D^{*-} \Lambda_c^+$  [65], and  $J/\psi n$  [66, 67]. The hidden-hadron production channels ( $\phi n$ ,  $J/\psi n$ ) are found to be more suppressed than the corresponding open-hadron production channels ( $K^{*0} \Lambda$ ,  $D^{*-} \Lambda_c^+$ ) due to the Okubo-Zweig-Iizuka (OZI) rule [68–70], similar to the kaon-induced reactions shown in Fig. 10(a). The predicted cross section for the  $D^{*-} \Lambda_c^+$  channel is in good agreement with the available experimental upper limit [65]. The peak structure observed in the  $\pi^- p \rightarrow J/\psi n$  reaction originates from the contributions of the hidden-charm pentaquark states  $P_c(4380)$  and  $P_c(4450)$  [71]. The resulting cross section near threshold is close to the experimental upper limit [66, 67]. Note that the result for the  $J/\psi n$  production should be regarded as a lower bound on the cross section, since only the summed branching ratio  $\mathcal{B}(\phi \rightarrow \rho\pi + \pi^+ \pi^- \pi^0) = 15.32\%$  is experimentally available [49]. This leads to an ambiguity in determining the individual  $\mathcal{B}(\phi \rightarrow \rho\pi)$  channel.

Figure 11 displays the predicted  $t$ -dependent differential cross sections for the  $K^- p \rightarrow D_s^{*-} \Lambda_c^+$  and  $K^- p \rightarrow J/\psi\Lambda$  reactions at four fixed beam energies. As expected, forward peaks are observed in both cases, particularly in the latter case. The differential cross sections are expressed in units of  $\text{nb}/\text{GeV}^2$  and  $\text{pb}/\text{GeV}^2$ , respectively. Consequently, future high-precision accelerator facilities will be required to measure such small cross sections, particularly for the latter reaction.

In Fig. 12, we show the individual predictions for the SDMEs as functions of  $-t'$  at  $P_{\text{Lab}} = 15$  GeV in both the helicity and GJ frames. In principle, for the vector-meson Reggeon exchange, the matrix elements  $\rho_{\lambda\lambda'}$  with  $|\lambda| = |\lambda'| = 1$  are specifically enhanced. This behavior

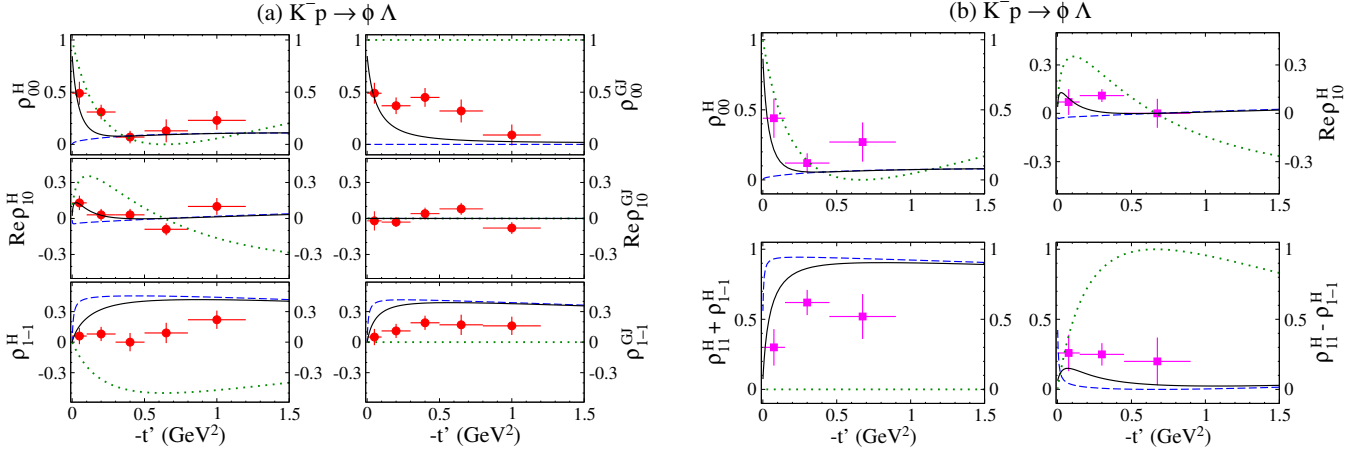


FIG. 8. SDMEs for the  $K^- p \rightarrow \phi \Lambda$  reaction as functions of  $-t'$ . (a)  $\rho_{00}$ ,  $\text{Re} \rho_{10}$ , and  $\rho_{1-1}$  in the helicity and GJ frames at  $P_{\text{Lab}} = 4.2 \text{ GeV}$ . (b)  $\rho_{00}$ ,  $\text{Re} \rho_{10}$ , and  $\rho_{11} \pm \rho_{1-1}$  in the helicity frame at  $P_{\text{Lab}} = 5 \text{ GeV}$ . Experimental data are taken from Refs. [31] (circles) and [30] (squares). Curve notations are the same as in Fig. 5.

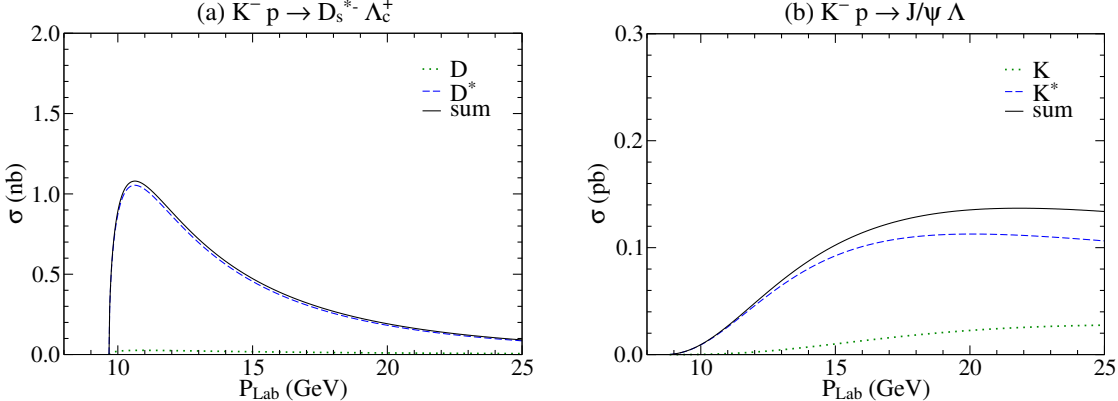


FIG. 9. Total cross sections for the (a)  $K^- p \rightarrow D_s^{*-} \Lambda_c^+$  and (b)  $K^- p \rightarrow J/\psi \Lambda$  reactions as functions of  $P_{\text{Lab}}$ . The green dotted and blue dashed curves denote the contributions from pseudoscalar- and vector-Reggeon exchanges, respectively, while the black solid curve represents their sum.

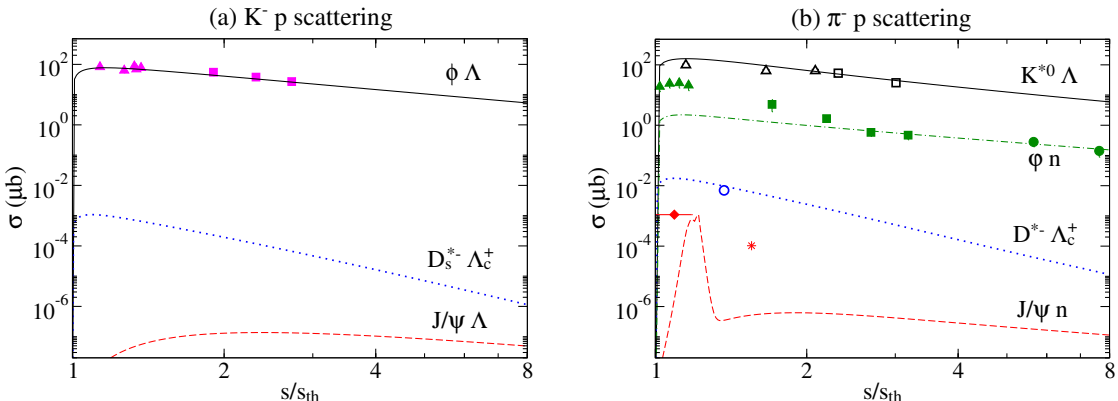


FIG. 10. (a) Total cross sections for the reactions  $K^- p \rightarrow (\phi \Lambda, D_s^{*-} \Lambda_c^+, J/\psi \Lambda)$  as functions of  $s/s_{\text{th}}$ . Experimental data are taken from Refs. [29] (triangles) and [30] (squares). (b) Total cross sections for the reactions  $\pi^- p \rightarrow (K^{*0} \Lambda, \phi n, D^{*-} \Lambda_c^+, J/\psi n)$ . Experimental data are taken from Refs. [63] (open triangles), [61] (open squares), [64] (triangles), [30] (squares and circles), [65] (open circles), [66] (diamonds), and [67] (stars). Theoretical results are taken from Refs. [15, 18].

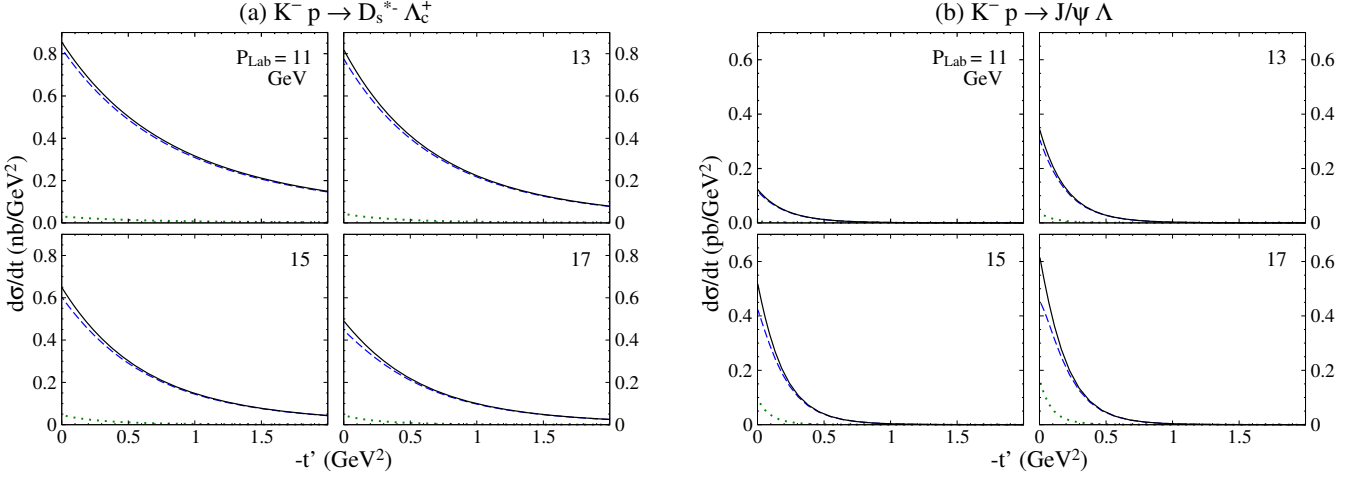


FIG. 11.  $t$ -dependent differential cross sections for the (a)  $K^- p \rightarrow D_s^{*-} \Lambda_c^+$  and (b)  $K^- p \rightarrow J/\psi \Lambda$  reactions at four fixed beam energies. Curve notations are the same as in Fig. 9.

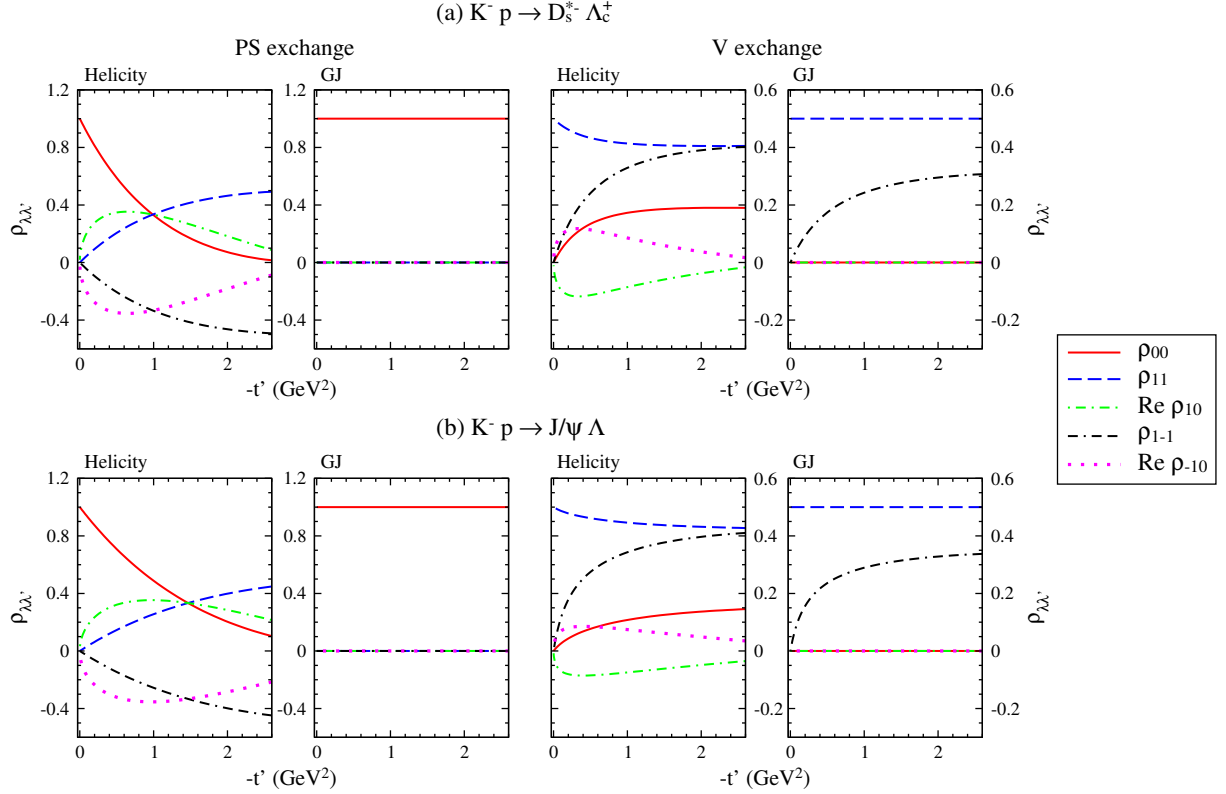


FIG. 12. SDMEs for the (a)  $K^- p \rightarrow D_s^{*-} \Lambda_c^+$  and (b)  $K^- p \rightarrow J/\psi \Lambda$  reactions as functions of  $-t'$  at  $P_{\text{Lab}} = 15$  GeV. The results for pseudoscalar- and vector-Reggeon exchanges are shown in the left and right panels, respectively, in both the helicity and GJ frames.

originates from the spin structure  $\epsilon^{\mu\nu\alpha\beta}\epsilon_\mu^*(\lambda_V)k_{2\alpha}k_{1\beta}$  of the amplitude in Eq. (9). In the vector meson rest frame, where  $\mathbf{k}_2 = (M_V, 0, 0, 0)$  and  $\mathbf{k}_1$  corresponds to the incoming kaon three-momentum  $\mathbf{p}_K$ , this factor is proportional to the vector product  $\epsilon^*(\lambda_V) \times \mathbf{p}_K$ . In the helicity frame and at small momentum transfers,  $\mathbf{p}_K$  has a large  $z$  component and a small transverse component, which yields  $\epsilon^*(\lambda_V) \times \mathbf{p}_K \simeq i\lambda_V \epsilon^*(\lambda_V) |\mathbf{p}_K|$ , thereby leading to a pronounced enhancement of  $\rho_{|\lambda|=1, |\lambda'|=1}$ . In the GJ frame,  $\mathbf{p}_K$  is aligned with the quantization axis;

it has a small  $z$  component and a large transverse component, which yields  $\epsilon^*(\lambda_V) \times \mathbf{p}_K \simeq 0$ , thereby leading to a suppression of  $\rho_{|\lambda|=1, |\lambda'|=1}$ .

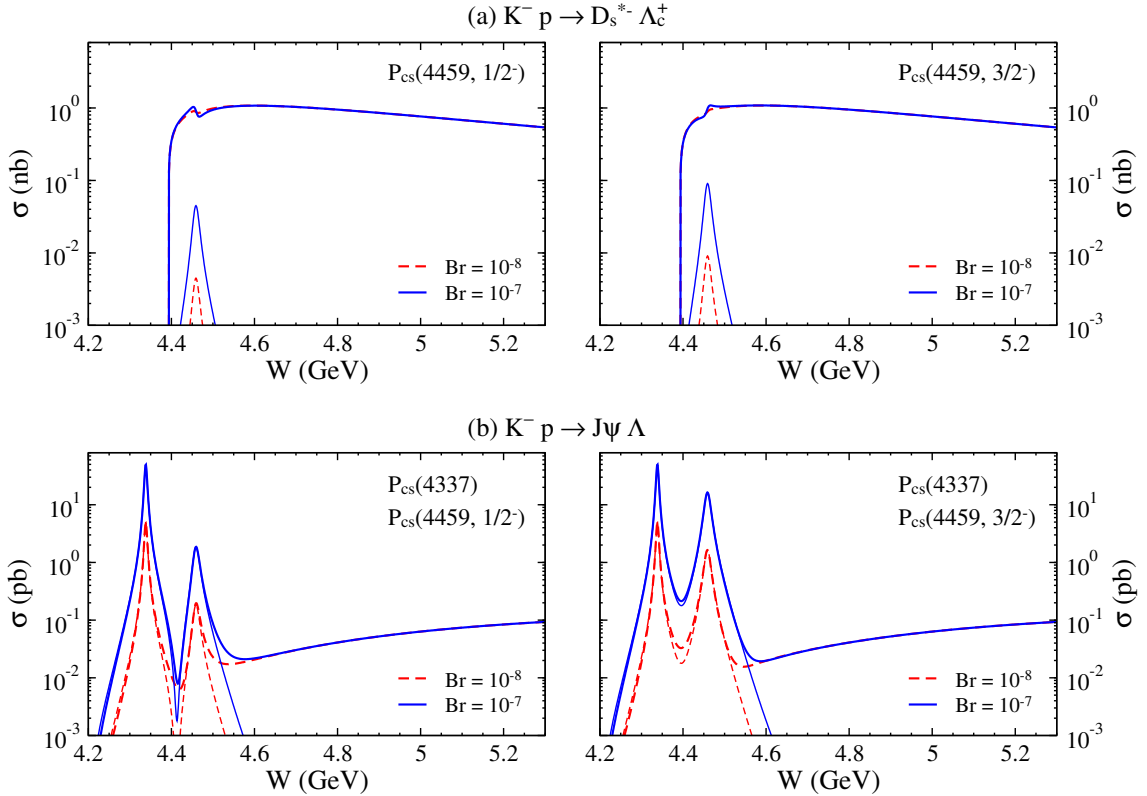


FIG. 13. Total cross sections for the (a)  $K^- p \rightarrow D_s^{*-} \Lambda_c^+$  and (b)  $K^- p \rightarrow J/\psi \Lambda$  reactions as functions of  $W$ , including contributions from the  $P_{cs}(4337)^0$  and  $P_{cs}(4459)^0$  states. Left and right panels correspond to  $J^P = 1/2^-$  and  $3/2^-$  for  $P_{cs}(4459)^0$ , respectively. The branching ratio  $\mathcal{B}(P_{cs} \rightarrow \bar{K}N)$  is taken to be  $10^{-7}$  and  $10^{-8}$ .

consequently,  $\rho_{\lambda\lambda'}$  vanishes whenever either  $\lambda = 0$  or  $\lambda' = 0$ . For the pseudoscalar-Reggeon exchange, however, the situation is markedly different. In this case, the scattering amplitude is proportional to the scalar product  $\boldsymbol{\varepsilon}^*(\lambda_V) \cdot \mathbf{p}_K$  in Eq. (9), which strongly enhances  $\rho_{00}$  in the GJ frame, so that  $\rho_{00} = 1$ , while all other  $\rho_{\lambda\lambda'}$  vanish [22].

### C. Pentaquark contributions to $K^- p \rightarrow D_s^{*-} \Lambda_c^+, J/\psi \Lambda$

Since we obtained reasonable estimates for the background contributions to the  $K^- p \rightarrow D_s^{*-} \Lambda_c^+$  and  $K^- p \rightarrow J/\psi \Lambda$  reactions in the previous subsection, we now investigate the  $s$ -channel  $P_{cs}$  contributions illustrated in Fig. 4. Using the branching ratios  $\mathcal{B}(P_{cs} \rightarrow \bar{D}_s^* \Lambda_c)$  and  $\mathcal{B}(P_{cs} \rightarrow J/\psi \Lambda)$  determined in Eqs. (32) and (33), we take the branching ratios for  $P_{cs} \rightarrow KN$  to be  $10^{-7}$  and  $10^{-8}$ , treating them as free parameters. The predicted total cross sections are shown in Fig. 13 as functions of the c.m. energy  $W = \sqrt{s}$ , where the results for  $P_{cs}(4459)^0$  with  $J^P = 1/2^-$  and  $3/2^-$  are displayed in the left and right panels, respectively. The contribution from the  $P_{cs}$  state with  $J^P = 3/2^-$  is larger than that with  $J^P = 1/2^-$  for both reactions. Since the background

contribution to the (a)  $K^- p \rightarrow D_s^{*-} \Lambda_c^+$  reaction is much larger than that to the (b)  $K^- p \rightarrow J/\psi \Lambda$  reaction, the  $P_{cs}(4459)^0$  signal is difficult to observe in the  $D_s^{*-} \Lambda_c^+$  channel. In contrast, both  $P_{cs}(4337)^0$  and  $P_{cs}(4459)^0$  give sizable contributions to  $J/\psi \Lambda$  production, with the contribution from  $P_{cs}(4337)^0$  being larger.

## IV. SUMMARY AND CONCLUSION

In this work, we investigated strangeness production in the  $K^- p \rightarrow \phi \Lambda$  reaction within a hybrid Regge framework. The reaction dynamics are found to be governed predominantly by  $t$ -channel exchanges. In particular, the  $K^*$ -Reggeon exchange provides the leading contribution over the considered energy range, while the  $K$ -Reggeon exchange plays a nonnegligible role, especially in reproducing the observed SDMEs. Contributions from the  $s$ -channel  $\Lambda$  and  $u$ -channel nucleon exchanges turn out to be strongly suppressed.

Extending the same Regge-based approach, we analyzed the open-charm  $K^- p \rightarrow D_s^{*-} \Lambda_c^+$  and hidden-charm  $K^- p \rightarrow J/\psi \Lambda$  reactions within a QGSM-motivated framework. The Regge trajectories  $\alpha(t)$  and energy-scale parameters  $s_0$  were determined consistently, thereby reducing model dependence and theoretical uncertain-

ties. Our results indicate that the production rates for the open- and hidden-charm channels are strongly suppressed, by roughly 5–6 and 8–9 orders of magnitude, respectively, compared with the strangeness-production channel, depending on the kinematical region. This strong suppression originates mainly from the larger energy-scale parameters and much smaller effective coupling strengths in the charm sector.

We further explored possible  $s$ -channel contributions from the hidden-charm pentaquark states with strangeness,  $P_{cs}(4337)^0$  and  $P_{cs}(4459)^0$ . While their effects are difficult to isolate in the open-charm channel due to the large nonresonant background, they may produce noticeable enhancements in the  $J/\psi\Lambda$  channel, suggesting that hidden-charm production could provide a more favorable environment for studying the  $P_{cs}$  states.

Other reaction mechanisms, such as scalar  $\kappa$  and axial-vector  $K_1$  exchanges, are in principle possible for the  $K^-p \rightarrow \phi\Lambda$  reaction but were not included in the present work, since their contributions are expected to be small compared with those of the  $K$ - and  $K^*$ -Reggeon exchanges. In addition, the tetraquark candidate  $Z_{cs}(4000)^+$ , observed in the  $J/\psi K^+$  channel and having a possible  $c\bar{c}u\bar{s}$  quark content [72], could contribute to the  $K^-p \rightarrow J/\psi\Lambda$  reaction via  $t$ -channel exchange. Such effects were also not considered here and

deserve further study.

Our predictions for charm-production observables, including total and differential cross sections as well as SDMEs, can serve as useful benchmarks for future measurements at J-PARC [2, 27, 28]. Within the same theoretical framework, the present study can be extended to other strangeness and charm production processes in kaon-induced reactions, such as  $K^-p \rightarrow \phi\Sigma^0$ ,  $D_s^{*-}\Sigma_c^+$ ,  $J/\psi\Sigma^0$ , as well as to pion-induced reactions like  $\pi^-p \rightarrow K^{*0}\Sigma^0$ ,  $D^{*0}\Sigma_c^0$ . The positive-parity states  $D_{s0}(2317)$  and  $D_{s1}(2460)$  lie about 40 MeV below the  $DK$  and  $D^*K$  thresholds, respectively, and are widely discussed in connection with  $DK$  and  $D^*K$  molecular interpretations [73, 74]. It is therefore interesting to investigate their production mechanisms in the  $K^-p \rightarrow D_{s0}(2317)\Lambda_c^+$  and  $K^-p \rightarrow D_{s1}(2460)\Lambda_c^+$  reactions [75]. Such studies may provide further insight into their internal structure and underlying dynamics. Working along these lines is currently in progress.

## ACKNOWLEDGMENTS

The work was supported by the Basic Science Research Program through the National Research Foundation of Korea (NRF) under Grants No. RS-2021-NR060129.

---

[1] M. F. M. Lutz *et al.* (PANDA Collaboration), Physics performance report for PANDA: Strong interaction studies with antiprotons, [arXiv:0903.3905 \[hep-ex\]](https://arxiv.org/abs/0903.3905).

[2] K. Aoki *et al.*, Extension of the J-PARC hadron experimental facility: Third White Paper, [arXiv:2110.04462 \[nucl-ex\]](https://arxiv.org/abs/2110.04462).

[3] M. Andreotti *et al.*, Results of a search for the  $h_c(^1P_1)$  state of charmonium in the  $\eta_c\gamma$  and  $J/\psi\pi^0$  decay modes, *Phys. Rev. D* **72**, 032001 (2005).

[4] B. Singh *et al.* (PANDA Collaboration), Feasibility study for the measurement of  $\pi N$  transition distribution amplitudes at PANDA in  $\bar{p}p \rightarrow J/\psi\pi^0$ , *Phys. Rev. D* **95**, 032003 (2017).

[5] J. Haidenbauer and G. Krein, Production of charmed pseudoscalar mesons in antiproton-proton annihilation, *Phys. Rev. D* **89**, 114003 (2014).

[6] J. Haidenbauer and G. Krein, Production of charmed baryons in  $\bar{p}p$  collisions close to their thresholds, *Phys. Rev. D* **95**, 014017 (2017).

[7] A. I. Titov and B. Kampfer, Exclusive charm production in  $\bar{p}p$  collisions at  $\sqrt{s} \lesssim 15$  GeV, *Phys. Rev. C* **78**, 025201 (2008).

[8] R. Shyam and H. Lenske, Reaction  $\bar{p}p \rightarrow \bar{\Lambda}_c^-\Lambda_c^+$  within an effective Lagrangian model, *Phys. Rev. D* **90**, 014017 (2014).

[9] T. Sangkhakrit, S. I. Shim, Y. Yan, and A. Hosaka, Charmed baryon pair production in proton-antiproton collisions in effective Lagrangian and Regge approaches, *Eur. Phys. J. A* **58**, 32 (2022).

[10] G. T. Bodwin, E. Braaten, and G. P. Lepage, Rigorous QCD analysis of inclusive annihilation and production of heavy quarkonium, *Phys. Rev. D* **51**, 1125(1995); **55**, 5853(E) (1997).

[11] A. Lundborg, T. Barnes, and U. Wiedner, Charmonium production in  $p\bar{p}$  annihilation: Estimating cross sections from decay widths, *Phys. Rev. D* **73**, 096003 (2006).

[12] T. Barnes and X. Li, Associated charmonium production in low energy  $p\bar{p}$  annihilation, *Phys. Rev. D* **75**, 054018 (2007). [[arXiv:hep-ph/0611340 \[hep-ph\]](https://arxiv.org/abs/hep-ph/0611340)].

[13] H. Noumi *et al.*, J-PARC Hadron Experimental Facility Proposal P50, “Charmed baryon spectroscopy via the  $(\pi^-, D^{*-})$  reaction”, available at <https://j-parc.jp/researcher/Hadron/en/Proposal.e.html> (2012).

[14] S. H. Kim, A. Hosaka, H. C. Kim, H. Noumi, and K. Shiratori, Pion induced reactions for charmed baryons, *PTEP* **2014**, 103D01 (2014).

[15] S. H. Kim, A. Hosaka, H. C. Kim, and H. Noumi, Production of strange and charmed baryons in pion induced reactions, *Phys. Rev. D* **92**, 094021 (2015).

[16] S. I. Shim, A. Hosaka, and H. C. Kim, Heavy baryon production with an instanton interaction, *PTEP* **2020**, 053D01 (2020).

[17] S. Y. Ryu *et al.*, J-PARC Hadron Experimental Facility Proposal P111, “ $J/\psi$  production in  $\pi^-p$  reaction near threshold”, available at <https://j-parc.jp/researcher/Hadron/en/Proposal.e.html> (2025).

[18] S. H. Kim, H. Ch. Kim, and A. Hosaka, Heavy pentaquark states  $P_c(4380)$  and  $P_c(4450)$  in the  $J/\psi$  production induced by pion beams off the nucleon, *Phys. Lett. B* **763**, 358 (2016).

[19] A. Sibirtsev and K. Tsushima,  $J/\psi$  production in  $\pi N$  collisions, [arXiv:nucl-th/9810029 \[nucl-th\]](https://arxiv.org/abs/nucl-th/9810029).

[20] J. J. Wu and T. S. H. Lee, Production of  $J/\psi$  on the nucleon and on deuteron targets, *Phys. Rev. C* **88**, 015205 (2013).

[21] S. H. Kim, H. Ch. Kim, and A. Hosaka,  $K^0\Lambda$  and  $D^-\Lambda_c^+$  production induced by pion beams off the nucleon, *Phys. Rev. D* **94**, 094025 (2016).

[22] S. H. Kim, Y. Oh, and A. I. Titov, Decay angular distributions of  $K^*$  and  $D^*$  vector mesons in pion-nucleon scattering, *Phys. Rev. C* **95**, 055206 (2017).

[23] A. B. Kaidalov, Hadronic mass relations from topological expansion and string model, *Z. Phys. C* **12**, 63 (1982).

[24] K. G. Boreskov and A. B. Kaidalov, Production of charmed baryons in hadron-hadron collisions, *Yad. Fiz.* **37**, 174 (1983); [Sov. J. Nucl. Phys. **37**, 100 (1983)].

[25] A. B. Kaidalov and O. I. Piskunova, Production of charmed particles in the quark-gluon string model, *Yad. Fiz.* **43**, 1545 (1986); [Sov. J. Nucl. Phys. **43**, 994 (1986)].

[26] A. B. Kaidalov and P. E. Volkovitsky, Binary reactions in  $\bar{p}p$  collisions at intermediate energies, *Z. Phys. C* **63**, 517 (1994).

[27] T. Takahashi *et al.*, Beam and SKS spectrometers at the K1.8 beam line, *PTEP* **2012**, 02B010 (2012).

[28] K. Agari *et al.*, The K1.8BR spectrometer system at J-PARC, *PTEP* **2012**, 02B011 (2012).

[29] J. S. Lindsey and G. A. Smith, Production properties and decay modes of the  $\phi$  meson, *Phys. Rev.* **147**, 913 (1966).

[30] D. S. Ayres, R. Diebold, A. F. Greene, S. L. Kramer, J. S. Levine, A. J. Pawlicki, and A. B. Wicklund,  $\phi$ -meson production in  $\pi^-p$  and  $K^-p$  interactions from 3 to 6 GeV/c, *Phys. Rev. Lett.* **32**, 1463 (1974).

[31] M. Aguilar-Benitez, S. U. Chung, R. L. Eisner, and N. P. Samios, Study of nonstrange mesons produced in  $K^-p$  interactions at 3.9 and 4.6 GeV/c, *Phys. Rev. D* **6**, 29 (1972).

[32] R. Aaij *et al.* (LHCb Collaboration), Evidence of a  $J/\psi\Lambda$  structure and observation of excited  $\Xi^-$  states in the  $\Xi_b^- \rightarrow J/\psi\Lambda K^-$  decay, *Sci. Bull.* **66**, 1278 (2021).

[33] R. Aaij *et al.* (LHCb Collaboration), Evidence for a new structure in the  $J/\psi p$  and  $J/\psi\bar{p}$  systems in  $B_s^0 \rightarrow J/\psi p\bar{p}$  decays, *Phys. Rev. Lett.* **128**, 062001 (2022).

[34] R. Aaij *et al.* (LHCb Collaboration), Observation of a  $J/\psi\Lambda$  resonance consistent with a strange pentaquark candidate in  $B^- \rightarrow J/\psi\Lambda\bar{p}$  decays, *Phys. Rev. Lett.* **131**, 031901 (2023).

[35] B. Wang, L. Meng, and S. L. Zhu, Spectrum of the strange hidden charm molecular pentaquarks in chiral effective field theory, *Phys. Rev. D* **101**, 034018 (2020).

[36] F. Z. Peng, M. J. Yan, M. Sánchez Sánchez, and M. P. Pavon Valderrama, The  $P_{cs}(4459)$  pentaquark from a combined effective field theory and phenomenological perspective, *Eur. Phys. J. C* **81**, 666 (2021).

[37] R. Chen, Can the newly reported  $P_{cs}(4459)$  be a strange hidden-charm  $\Xi_c\bar{D}^*$  molecular pentaquark?, *Phys. Rev. D* **103**, 054007 (2021).

[38] F. L. Wang and X. Liu, Emergence of molecular-type characteristic spectrum of hidden-charm pentaquark with strangeness embodied in the  $P_{\psi s}^\Lambda(4338)$  and  $P_{cs}(4459)$ , *Phys. Lett. B* **835**, 137583 (2022).

[39] M. J. Yan, F. Z. Peng, M. Sánchez Sánchez, and M. Pavon Valderrama,  $P_{\psi s}^\Lambda(4338)$  pentaquark and its partners in the molecular picture, *Phys. Rev. D* **107**, 7 (2023).

[40] F. L. Wang, S. Q. Luo, H. Y. Zhou, Z. W. Liu, and X. Liu, Exploring the electromagnetic properties of the  $\Xi_c^{(',*)}\bar{D}_s^{(*)}$  and  $\Omega_c^{(*)}\bar{D}_s^{(*)}$  molecular states, *Phys. Rev. D* **108**, 034006 (2023).

[41] J. T. Zhu, S. Y. Kong, and J. He,  $P_{\psi s}^\Lambda(4459)$  and  $P_{\psi s}^\Lambda(4338)$  as molecular states in  $J/\psi\Lambda$  invariant mass spectra, *Phys. Rev. D* **107**, 034029 (2023).

[42] A. Feijoo, W. F. Wang, C. W. Xiao, J. J. Wu, E. Oset, J. Nieves, and B. S. Zou, A new look at the  $P_{cs}$  states from a molecular perspective, *Phys. Lett. B* **839**, 137760 (2023).

[43] F. L. Wang and X. Liu, Surveying the mass spectra and the electromagnetic properties of the  $\Xi_c^{(',*)}D^{(*)}$  molecular pentaquarks, *Phys. Rev. D* **109**, 1 (2024).

[44] B. Wang, K. Chen, L. Meng, and S. L. Zhu, Spectrum of the molecular pentaquarks, *Phys. Rev. D* **109**, 074035 (2024).

[45] L. Roca, J. Song, and E. Oset, Molecular pentaquarks with hidden charm and double strangeness, *Phys. Rev. D* **109**, 094005 (2024).

[46] Z. Y. Yang, F. Z. Peng, M. J. Yan, M. Sánchez Sánchez, and M. Pavon Valderrama, Molecular  $P_\psi$  pentaquarks from light-meson exchange saturation, *Phys. Rev. D* **111**, 014012 (2025).

[47] R. Chen, Strong decays of the newly  $P_{cs}(4459)$  as a strange hidden-charm  $\Xi_c\bar{D}^*$  molecule, *Eur. Phys. J. C* **81**, 122 (2021).

[48] C. W. Xiao, J. J. Wu, and B. S. Zou, Molecular nature of  $P_{cs}(4459)$  and its heavy quark spin partners, *Phys. Rev. D* **103**, 054016 (2021).

[49] S. Navas, *et al.*, Particle Data Group, *Phys. Rev. D* **110**, 030001 (2024).

[50] Y. Oh, K. Nakayama, and T. S. H. Lee, Pentaquark  $\theta^+(1540)$  production in  $\gamma N \rightarrow K\bar{K}N$ , *Phys. Rept.* **423**, 49 (2006).

[51] S. H. Kim, J. K. Ahn, Sh. H. Kim, S. i. Nam, and M. K. Cheoun, Double-strangeness exchange reactions in a hybrid Regge-plus-resonance approach, *Phys. Rev. C* **107**, 065202 (2023).

[52] T. A. Rijken, V. G. J. Stoks, and Y. Yamamoto, Soft-core hyperon-nucleon potentials, *Phys. Rev. C* **59**, 21 (1999).

[53] V. G. J. Stoks and T. A. Rijken, Soft-core baryon-baryon potentials for the complete baryon octet, *Phys. Rev. C* **59**, 3009 (1999).

[54] M. M. Brisudova, L. Burakovsky, and J. T. Goldman, Effective functional form of Regge trajectories, *Phys. Rev. D* **61**, 054013 (2000).

[55] P. Colangelo, F. De Fazio, and T. N. Pham, Nonfactorizable contributions in  $B$  decays to charmonium: The case of  $B^- \rightarrow K^-h_c$ , *Phys. Rev. D* **69**, 054023 (2004).

[56] F. K. Guo, C. Hanhart, G. Li, U. G. Meissner, and Q. Zhao, Effect of charmed meson loops on charmonium transitions, *Phys. Rev. D* **83**, 034013 (2011).

[57] J. X. Lu, M. Z. Liu, R. X. Shi, and L. S. Geng, Understanding  $P_{cs}(4459)$  as a hadronic molecule in the  $\Xi_b^- \rightarrow J/\psi\Lambda K^-$  decay, *Phys. Rev. D* **104**, 034022 (2021).

[58] X. W. Wang and Z. G. Wang, Strong decays of  $P_{cs}(4338)$  and its high isospin cousin via QCD sum rules, *Phys. Rev. D* **110**, 014008 (2024).

[59] S. H. Kim, Y. Oh, S. Son, S. Sakinah, and M. K. Cheoun, Effective Lagrangian for strong and electromagnetic interactions of high-spin resonances, *Phys. Rev. D* **111**, 054031 (2025).

- [60] K. Schilling, P. Seyboth, and G. E. Wolf, On the analysis of vector meson production by polarized photons, *Nucl. Phys. B* **15**, 397; **18**, 332(E) (1970).
- [61] D. J. Crennell, H. A. Gordon, K. W. Lai, and J. M. Scarr, Two-body strange-particle final states in  $\pi^- p$  interactions at 4.5 and 6 GeV/c, *Phys. Rev. D* **6**, 1220 (1972).
- [62] S. Clymton, H. J. Kim, and H. C. Kim, Production of hidden-charm strange pentaquarks  $P_{cs}$  from the  $K^- p \rightarrow J/\psi \Lambda$  reaction, *Phys. Rev. D* **104**, 014023 (2021).
- [63] O. I. Dahl, L. M. Hardy, R. I. Hess, J. Kirz, and D. H. Miller, Strange-particle production in  $\pi^- p$  interactions from 1.5 to 4.2 BeV/c. 1. Three-and-more-body final states, *Phys. Rev. D* **163**, 1377 (1967).
- [64] H. Courant, Y. I. Makdisi, M. L. Marshak, E. A. Peterson, K. Ruddick, and J. Smith-Kintner,  $\phi$  production in  $\pi^- p$  collisions near threshold, *Phys. Rev. D* **16**, 1 (1977).
- [65] J. H. Christenson, E. Hummel, G. A. Kreiter, J. Sculli, and P. Yamin, Limits on charm production in hadronic interactions near threshold, *Phys. Rev. Lett.* **55**, 154 (1985).
- [66] K. Jenkins *et al.*, A search for the reaction  $\pi^- p \rightarrow \psi n$  near threshold, *Phys. Rev. D* **17**, 52 (1978).
- [67] I. H. Chiang *et al.*, Search for exclusive  $J/\psi$  production, *Phys. Rev. D* **34**, 1619 (1986)
- [68] S. Okubo,  $\phi$ -meson and unitary symmetry model, *Phys. Lett.* **5**, 165 (1963).
- [69] G. Zweig, CERN Reports, CERN-TH-401 and CERN-TH-412, 1964.
- [70] J. Iizuka, Systematics and phenomenology of meson family, *Prog. Theor. Phys. Suppl.* **37**, 21 (1966).
- [71] R. Aaij *et al.* (LHCb Collaboration), Observation of  $J/\psi p$  resonances consistent with pentaquark states in  $\Lambda_b^0 \rightarrow J/\psi K^- p$  decays, *Phys. Rev. Lett.* **115**, 072001 (2015).
- [72] R. Aaij *et al.* (LHCb Collaboration), Observation of new resonances decaying to  $J/\psi K^+$  and  $J/\psi \phi$ , *Phys. Rev. Lett.* **127**, 082001 (2021).
- [73] A. Faessler, T. Gutsche, V. E. Lyubovitskij, and Y. L. Ma,  $D^* K$  molecular structure of the  $D_{s1}(2460)$  meson, *Phys. Rev. D* **76**, 114008 (2007).
- [74] L. Liu, K. Orginos, F. K. Guo, C. Hanhart, and U. G. Meissner, Interactions of charmed mesons with light pseudoscalar mesons from lattice QCD and implications on the nature of the  $D_{s0}^*(2317)$ , *Phys. Rev. D* **87**, 014508 (2013).
- [75] H. Zhu and Y. Huang, Production of the  $D_{s0}(2317)$  and  $D_{s1}(2460)$  by kaon-induced reactions on a proton target, *Phys. Rev. D* **100**, 054031 (2019).